

# UC Santa Barbara

## UC Santa Barbara Previously Published Works

### Title

Baseline unfolded protein response signaling adjusts the timing of the mammalian cell cycle.

### Permalink

<https://escholarship.org/uc/item/9cq1q81g>

### Journal

Cell regulation, 35(6)

### Authors

Chowdhury, Soham

Solley, Sabrina

Polishchuk, Elena

et al.

### Publication Date

2024-06-01

### DOI

10.1091/mbc.E23-11-0419

### Copyright Information

This work is made available under the terms of a Creative Commons Attribution License, available at <https://creativecommons.org/licenses/by/4.0/>

Peer reviewed

# Baseline unfolded protein response signaling adjusts the timing of the mammalian cell cycle

Soham P. Chowdhury<sup>a,†</sup>, Sabrina C. Solley<sup>a,†,‡</sup>, Elena Polishchuk<sup>b</sup>, Julien Bacal<sup>a</sup>, Julia E. Conrad<sup>c</sup>, Brooke M. Gardner<sup>a</sup>, Diego Acosta-Alvear<sup>a,§,\*</sup>, and Francesca Zappa<sup>b,¶,§,\*</sup>

<sup>a</sup>Department of Molecular, Cellular, and Developmental Biology, University of California, Santa Barbara, Santa Barbara, CA 93106; <sup>b</sup>Telethon Institute of Genetics and Medicine (TIGEM), 80078 Pozzuoli, Naples, Italy; <sup>c</sup>Altos Labs Bay Area Institute of Science, Altos Labs, Redwood City, CA 94065

**ABSTRACT** The endoplasmic reticulum (ER) is a single-copy organelle that cannot be generated *de novo*, suggesting coordination between the mechanisms overseeing ER integrity and those controlling the cell cycle to maintain organelle inheritance. The Unfolded Protein Response (UPR) is a conserved signaling network that regulates ER homeostasis. Here, we show that pharmacological and genetic inhibition of the UPR sensors IRE1, ATF6, and PERK in unstressed cells delays the cell cycle, with PERK inhibition showing the most penetrant effect, which was associated with a slowdown of the G<sub>1</sub>-to-S/G<sub>2</sub> transition. Treatment with the small molecule ISRIB to bypass the effects of PERK-dependent phosphorylation of the translation initiation factor eIF2 $\alpha$  had no such effect, suggesting that cell cycle timing depends on PERK's kinase activity but is independent of eIF2 $\alpha$  phosphorylation. Using complementary light and electron microscopy and flow cytometry-based analyses, we also demonstrate that the ER enlarges before mitosis. Together, our results suggest coordination between UPR signaling and the cell cycle to maintain ER physiology during cell division.

## Monitoring Editor

Guillaume Thibault  
Nanyang Technological  
University

Received: Nov 6, 2023

Revised: Apr 16, 2024

Accepted: Apr 17, 2024

## SIGNIFICANCE STATEMENT

- The endoplasmic reticulum (ER) is a single-copy organelle that cannot be generated *de novo*, and its functions are controlled by the Unfolded Protein Response (UPR). How the UPR impacts the cell cycle remained unclear.
- By investigating this connection, the authors describe distinct roles for each UPR sensor, with PERK activity significantly affecting cell cycle beyond its typical function in the Integrated Stress Response (ISR). They also show that the ER expands before mitosis, potentially linking ER expansion to partitioning during mitosis.
- These findings highlight an unexplored UPR function in cell cycle regulation, potentially serving as a critical checkpoint for mitosis.

This article was published online ahead of print in MBoC in Press (<http://www.molbiolcell.org/cgi/doi/10.1091/mbc.E23-11-0419>) on April 24, 2024.

<sup>†</sup>These authors contributed equally to this work and should be regarded as co-first authors.

<sup>‡</sup>Present addresses: Department of Molecular Biology, Princeton University, Princeton, NJ, 08544; <sup>§</sup>Altos Labs Bay Area Institute of Science, Altos Labs, Redwood City, CA, 94065.

Author Contributions: S.C., S.C.S., and F.Z. designed experiments, collected, and analyzed data. F.Z. conceived and designed the analyses. E.P. collected and analyzed TEM data. J.B. collected and analyzed EdU profiling data. J.E.C. engineered cell lines and collected data. B.M.G. and D.A.-A. supervised the research. S.P.C., S.C.S, F.Z., and D.A.-A. wrote the paper.

Author disclosures: D.A.-A. is an inventor in U.S. patent 9708247 held by the Regents of the University of California that describes ISRIB and its analogues. Rights

to the invention have been licensed to Calico Life Sciences LLC. J.E.C., D.A.-A. and F.Z. are employees of Altos Labs.

\*Address correspondence to: Diego Acosta-Alvear ([dacostaalvear@altoslabs.com](mailto:dacostaalvear@altoslabs.com)); Francesca Zappa ([fzappa@altoslabs.com](mailto:fzappa@altoslabs.com))

Abbreviations used:

© 2024 Chowdhury *et al.* This article is distributed by The American Society for Cell Biology under license from the author(s). It is available to the public under an Attribution 4.0 International Creative Commons CC-BY 4.0 License (<https://creativecommons.org/licenses/by/4.0/>).

"ASCB®," "The American Society for Cell Biology®," and "Molecular Biology of the Cell®" are registered trademarks of The American Society for Cell Biology.

## HIGHLIGHTS:

- Blocking the UPR sensors in unstressed cells affects cell cycle dynamics.
- PERK has cell cycle roles that are independent of phosphorylating eIF2 $\alpha$ .
- The ER expands during the mammalian cell cycle.

## INTRODUCTION

The mammalian cell cycle consists of four well-defined stages: Gap 1 (G<sub>1</sub>), Synthesis (S), Gap 2 (G<sub>2</sub>), and mitosis, that are coordinated through finely adjusted temporal control and cell-cycle checkpoints to ensure the correct inheritance of the genome and cellular components by the daughter cells. This coordination requires multiple signaling pathways to integrate information about genome and organelle integrity, and whether conditions for progression through the cell cycle are suitable (e.g., energy status and resource availability; Rhind and Russell, 2012; Barnum and O'Connell, 2014). Additionally, because cytokinesis requires cell growth, cells employ mechanisms to regulate their size and adjust cellular content to ensure correct organelle inheritance (Kuroiwa, 2010). This coordination of mechanisms is essential for organelle partitioning. While multicopy organelles such as mitochondria and peroxisomes tend to be partitioned symmetrically among daughter cells, some membrane-bound organelles, including the Golgi apparatus and the endoplasmic reticulum (ER), fragment during cell division, suggesting synchronization between organelle restructuring and the cell cycle (Thyberg and Moskalewski, 1998). Indeed, the partitioning of the Golgi apparatus during mitosis has been linked to the activity of the cell cycle kinases PKMYT1 and CDK1 (Nakajima *et al.*, 2008; Ayala and Colanzi, 2017; Huang *et al.*, 2022). Surprisingly, no such link has been described for the ER.

The ER is the largest organelle in the cell and the site of secreted and membrane protein biosynthesis, calcium storage, lipid synthesis, and endomembrane biogenesis (Voeltz and Prinz, 2007). The ER also possesses structural subdomains (e.g., sheets, tubules, ER exit sites, and ER-organelle membrane contact sites) and is distinctly organized in different cell types; while professional secretory cells show an enlarged rough ER, cells dedicated to lipid synthesis possess mostly tubular ER, reflecting their respective physiological roles (Shibata *et al.*, 2006, 2010). Moreover, because the ER is contiguous with the nuclear envelope, it maintains the separation of functions between the nucleoplasm and cytoplasm, otherwise topologically equivalent compartments (Dawson *et al.*, 2009; Walters *et al.*, 2012). The ER's complexity has led to contested models explaining its structure and reorganization during mitosis, with some studies suggesting complete vesiculation and disassembly, while others indicate the formation of fenestrated mitotic ER sheets (Cotter *et al.*, 2007; Puhka *et al.*, 2007). Although the mechanisms behind ER inheritance remain unclear, it is agreed that the ER undergoes structural changes before cell division.

Structural and functional rearrangements of the ER are handled by the UPR, an evolutionarily conserved signaling network that monitors and adjusts ER function to maintain ER homeostasis.

The mammalian UPR is governed by three ER-membrane sensors that detect ER protein-folding and ER membrane perturbations, collectively known as ER stress. These ER stress sensors are the kinase/RNase IRE1, the kinase PERK, and the membrane-tethered transcription factor ATF6 (Halbleib *et al.*, 2017; Tam *et al.*, 2018; Karagöz *et al.*, 2019; Fun and Thibault, 2020). Upon ER stress sensing, IRE1 and PERK self-associate, trans-autophosphorylate, and homo-oligomerize in the plane of the ER membrane. Active

IRE1 induces the transcription factor XBP1S (S for "spliced") through nonconventional splicing of the XBP1 mRNA and degrades a subset of mRNAs in a process known as regulated IRE1-dependent decay (RIDD; Hollien and Weissman, 2006). Active PERK phosphorylates the alpha subunit of the eukaryotic translation initiation factor 2 (eIF2 $\alpha$ ), leading to a global translational shutdown and the selective translation of some mRNAs, including the stress-responsive transcription factor ATF4 (Harding *et al.*, 2000a). ER stress causes ATF6 to traffic to the Golgi apparatus, wherein it undergoes regulated proteolysis to liberate its soluble transcription factor portion from the membrane (Yoshida *et al.*, 1998). Together, IRE1, PERK, and ATF6 induce gene expression and translational programs that restore ER homeostasis (Karagöz *et al.*, 2019). XBP1 and ATF6 also regulate lipid biosynthesis and endomembrane biogenesis, thereby controlling the volumetric expansion of the ER (Sriburi *et al.*, 2004; Bommasamy *et al.*, 2009). Because of its crucial role in ER maintenance, we reasoned the UPR could provide a long-sought house-keeping link between ER reorganization and the cell cycle that is reflective of cellular physiology.

## RESULTS

Because the UPR adjusts ER function and size, we hypothesized it could integrate ER physiology and the cell cycle. Indeed, an intact UPR is required for cytokinesis in budding yeast (Bicknell *et al.*, 2007), and, not surprisingly, activation of the UPR with ER poisons typically used in the laboratory inhibits cell cycle progression (Han *et al.*, 2013; Lee *et al.*, 2019). Nevertheless, the roles of the UPR in coordinating mammalian cell-cycle dynamics in unstressed cells remain unexamined. To address this knowledge gap, we manipulated the baseline UPR in unstressed H4 neuroglioma cells (i.e., without any acute stress induced by classical ER poisons used in the laboratory) and studied cell cycle progression. We inhibited IRE1's RNase activity with the aldehyde inhibitor 4 $\mu$ 8C; ATF6 with ceapin-A7, a small molecule that prevents ATF6's ER-to-Golgi trafficking and thus blocks its activation; and PERK with the kinase inhibitor GSK2606414 (Axten *et al.*, 2012; Cross *et al.*, 2012; Gallagher *et al.*, 2016). Because the ATF6 and IRE1-XBP1 transcriptional responses partially overlap and could be redundant (Lee *et al.*, 2003; Sriburi *et al.*, 2004; Shoulders *et al.*, 2013), we also tested a combination of 4 $\mu$ 8C and ceapin-A7. Because the UPR shares a sensor-PERK—with the integrated stress response (ISR), we also sought to exclude potential ISR-specific effects by treating cells with the potent ISR inhibitor ISRIB, which renders cells insensitive to the effects of eIF2 $\alpha$  phosphorylation (Sidrauski *et al.*, 2013).

Both 4 $\mu$ 8C and ceapin-A7 treatment reduced H4 cell proliferation over 7 d (Figure 1A), and the combination of 4 $\mu$ 8C and ceapin-A7 had an additive effect. To maintain drug efficacy during the time course and minimize potential effects resulting from changes in cell population density, we replenished the drugs every 24 h and, at the same time, we diluted and reseeded the cells and evaluated viability (see *Materials and Methods* for details). Surprisingly, although treatment with ISRIB was nonperturbative, GSK2606414 treatment led to a strong antiproliferative effect. Notably, none of the drugs substantially impaired cell viability in our experiments (Figure 1B), and thus, we infer that the antiproliferative effects we observed result from a delay of the cell cycle rather than induction of cell death. Moreover, a 4 d pretreatment with GSK2606414 followed by a 9-h pulse exposure to nocodazole to arrest cells in G<sub>2</sub> led to a modest, yet significant, decrease in the proportion of cells in G<sub>2</sub> compared with DMSO-treated control cells, as assessed by EdU pulse-labeling and EdU/PI flow cytometry profiling, while treatment with ISRIB

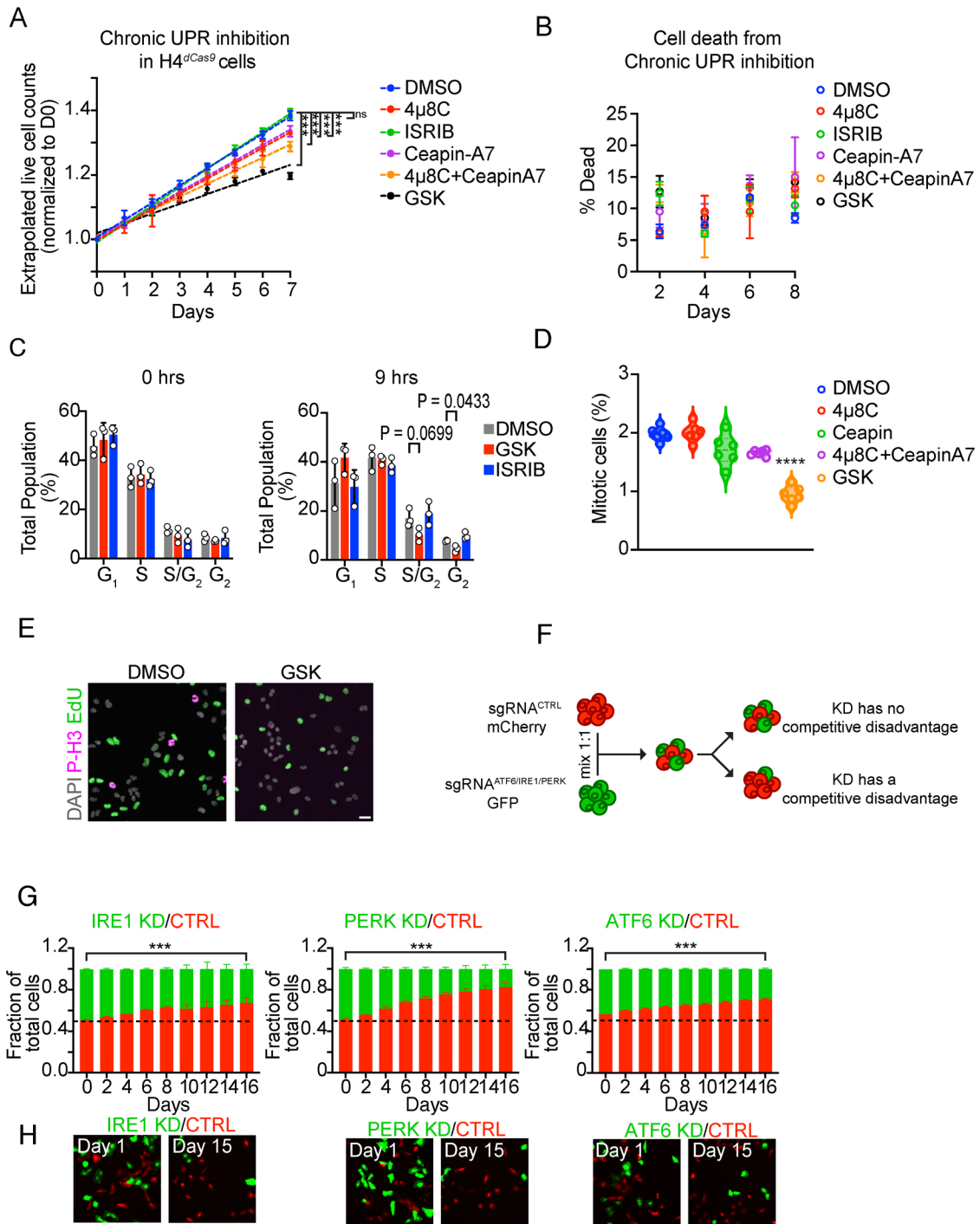


**FIGURE 1:** (A) Pharmacological inhibition of the UPR delays the growth of H4 CRISPRi cells ( $N = 3$ ; Paired two-tailed  $t$  test,  $***P < 0.001$ ,  $**P < 0.01$ ,  $*P < 0.05$ ). (B) Pharmacological UPR inhibition does not induce significant cell death in H4 CRISPRi cells over one week of treatment ( $N = 3$ ,  $P = n.s.$ , Paired two-tailed  $t$  test; see *Materials and Methods* for details). (C) EdU/PI cell cycle profile analysis of H4 CRISPRi cells treated with GSK2606414, ISRIB, or DMSO for 4 d (0 h; see *Materials and Methods* for details) and an additional 9 h in nocodazole to arrest cells in the G<sub>2</sub>/M boundary ( $N = 3$ , two-way ANOVA). (D) Quantification and analysis of mitotic cells upon 4 d of pharmacological UPR inhibition ( $N = 5$ ,  $n > 1377$ , 2-way ANOVA). (E) Representative images of the quantification in (D). Nuclei (DAPI) are shown in gray, cells stained for the mitotic marker phospho-histone-3 (P-H3) are shown in magenta, and cells stained for ethynyl-deoxyuridine (EdU), indicating DNA synthesis has occurred, are shown in green. Scale bar: 20  $\mu\text{m}$ . (F) Schematic of a cell competition assay for the ratiometric measurement of the impact of the genetic depletion of each UPR sensor in cell population dynamics. (G) Flow cytometry-based quantification of the proportions of GFP+ and mCherry+ cells in the cell competition assay depicted in (F). Representative micrographs are shown below ( $N = 3$ ; Paired two-tailed  $t$  test,  $***P < 0.001$ ,  $**P < 0.01$ ,  $*P < 0.05$ ).

showed no such effect (Red and blue bars compared with vehicle control grey bars at 9 h of nocodazole treatment; Figure 1C), suggesting that baseline PERK inhibition—but not ISR inhibition—delays the G<sub>1</sub> to S/G<sub>2</sub> transition. Analysis of mitotic cells in asynchronous populations where we inhibited the UPR sensors confirmed these observations, indicating significantly fewer cells in mitosis upon GSK2606414 treatment when compared with the control (Figure 1, D and E). Together, these results suggest that the UPR influences cell-cycle kinetics and, surprisingly, substantiate that PERK's kinase activity, but not eIF2 $\alpha$  phosphorylation, plays a significant role in cell cycle dynamics.

Recognizing the potential off-target effects of drugs, we set out to investigate the impact of genetic depletion of the UPR sensors on the cell cycle using a cell competition assay. We labeled H4 cells carrying the CRISPR interference (CRISPRi) machinery with GFP or mCherry. We introduced small guide RNAs (sgRNAs) targeting IRE1, PERK, or ATF6 into GFP-labeled cells, and a nontargeting (GAL4) sgRNA control into mCherry labeled cells (Figure 1F). We verified IRE1 and PERK knockdown efficiency by immunoblot, and ATF6 by qRT-PCR due to the lack of reliable antibodies (Supplemental Figure S1A). Next, we cocultured the GFP and mCherry expressing cells in a 1:1 ratio, diluted the mixed population every 48 h to maintain a constant seeding density, and analyzed the cells by flow cytometry and fluorescence microscopy at each interval. In line with our results with 4 $\mu$ 8C, ceapin-A7, and GSK2606414, cells depleted of IRE1, ATF6, and PERK showed a proliferative disadvantage, evidenced by a time-dependent enrichment of mCherry expressing cells (Figure 1G). Notably, the genetic depletion of the UPR sensors phenocopied the effects of the drugs, where depletion of IRE1 and ATF6 gave comparable phenotypes, while PERK depletion showed the most profound antiproliferative effect (Figure 1G), substantiating a baseline role for PERK in maintaining cell cycle dynamics.

Based on these results and considering that the UPR regulates ER expansion (Sriburi *et al.*, 2004; Bommasamy *et al.*, 2009; Tam *et al.*, 2018), we hypothesized coordination between the observed UPR actions and ER enlargement in preparation for cell division. To measure ER expansion, we separated G<sub>1</sub> or S/G<sub>2</sub> H4 neuroglioma cells or KMS11 multiple myeloma CRISPRi cells by FACS based on the expression of a fluorescent reporter of cell-cycle stages known as Fast-FUCCI. This reporter encodes two fluorescent proteins, mKusibaraOrange and mAzamiGreen, fused to degrons of the cell cycle licensing factors CDT1 and geminin, respectively. The turnover of these proteins during G<sub>1</sub> and G<sub>2</sub> allows live cell measurements of a fluorescent label shift dependent on cell-cycle progression (Koh *et al.*, 2017). We chose H4 and KMS11 because they represent distinct physiological reliance on ER functions; KMS11 cells arise from professional secretory cells and secrete immunoglobulin light chains, while H4 cells are of neural origin with no dedicated secretory products.

FACS analysis of synchronized Fast-FUCCI/CRISPRi H4 and KMS11 cell lines confirmed the validity of our reporter-based approach, as we recovered cells in distinct stages of the cell cycle (Figure 2A). Next, we separated asynchronous Fast-FUCCI/CRISPRi H4 and KMS11 cells based on G<sub>1</sub> (mKusibaraOrange+) and S/G<sub>2</sub> (mAzamiGreen+) reporter expression and analyzed their cell size and granularity by flow cytometry. These analyses revealed that S/G<sub>2</sub> cells were larger and more granular, as indicated by increased forward and side scatter, suggesting a gain in biomass and organellar content following genome duplication (Figure 2, B and C). We next analyzed the levels of the mRNAs encoding select ER chaperones and foldases (BiP, PDIA6, and calnexin), by qRT-PCR, in FACS-separated Fast-FUCCI/CRISPRi H4 and KMS11 cells. We found no

significant enrichment of these mRNAs in S/G<sub>2</sub> cells compared with G<sub>1</sub> cells (Figure 2D), while analysis of the corresponding proteins by immunostaining showed marked (H4) or modest (KMS11) increases in ER protein content in S/G<sub>2</sub> compared with G<sub>1</sub> (Figure 2, E and F). The discrepancy between mRNA and protein levels could stem from transient mRNA upregulation preceding G<sub>2</sub>, cell-cycle associated translational control, or differences in protein turnover. The differences in protein expression between cell lines may be linked to their intrinsic physiology, and we speculate that the myeloma cells may not need to enlarge an already expansive secretory apparatus before cell division.

Last, to investigate whether the increases in the protein levels of ER chaperones and foldases are concurrent with a volumetric ER expansion, we analyzed the ultrastructure of ER cisternae in G<sub>1</sub> and S/G<sub>2</sub> cells by transmission electron microscopy (TEM). To this end, we separated asynchronous H4 and KMS11 Fast-FUCCI/CRISPRi cells into G<sub>1</sub> and S/G<sub>2</sub> subpopulations by FACS and quantified ER cisternal volume in TEM micrographs. These analyses revealed a volumetric ER increase in S/G<sub>2</sub> cells compared with those in G<sub>1</sub>, indicating that the ER has undergone physical expansion by the time the cells reach G<sub>2</sub> (Figure 2, G and H). Consistent with our analyses of ER protein content, H4 cells showed a larger ER volumetric increase compared with KMS11 cells, supporting our interpretation of intrinsic differences in secretory capacity. These results demonstrate pervasive structural and biochemical remodeling of the ER accompanying genome duplication as cells progress from G<sub>1</sub> to G<sub>2</sub> and correlate with our observations of UPR involvement in the mammalian cell cycle.

## DISCUSSION

The coordination of mechanisms maintaining organelle integrity and the cell cycle is fundamental to preserving the fidelity of organelle inheritance during cell division. Our results show that blocking the UPR in unstressed cells delays cell cycle progression and that the ER undergoes dynamic changes as cells progress from G<sub>1</sub> to G<sub>2</sub>. Our combined observations suggest the UPR likely coordinates dynamic ER changes in preparation for cell division. Our data align with previous findings showing that the UPR is required for cytokinesis in budding yeast and that increased fatty acid biosynthesis occurs during the S phase (Bicknell *et al.*, 2007; Bommasamy *et al.*, 2009; Tam *et al.*, 2018; Merta *et al.*, 2021). From these published results and ours, it follows that the ability to expand the ER and its biosynthetic capacity is an inherent aspect of the mammalian cell cycle.

Considering that the UPR is the master surveillance system that adjusts the ER's physiological capacity, it is likely that a housekeeping function of the UPR may be required in cycling cells for making structural and functional ER adjustments concordant with cell division. Because all three branches of the UPR respond to lipid bilayer stress and the IRE1 and ATF6 branches regulate endomembrane biosynthesis, the UPR may be particularly important for the controlled expansion of the ER we observed (Sriburi *et al.*, 2004; Bommasamy *et al.*, 2009). In line with this notion, pharmacological and genetic inhibition of IRE1 and ATF6 delayed cell cycle progression, and their combined loss-of-function led to a more profound defect, indicating a functional redundancy that may be linked to ER expansion (Figure 1A). Surprisingly, the inhibition of IRE1 and ATF6, alone or in combination, did not amount to the extent of the effect we observed upon PERK inhibition, which suggests a housekeeping role for PERK in adjusting cell cycle timing that is inherently distinct from the potential cell cycle roles of IRE1 and ATF6.

The striking discrepancy between our results with ISRIB and PERK inhibition suggests that the baseline phosphorylation of eIF2 $\alpha$



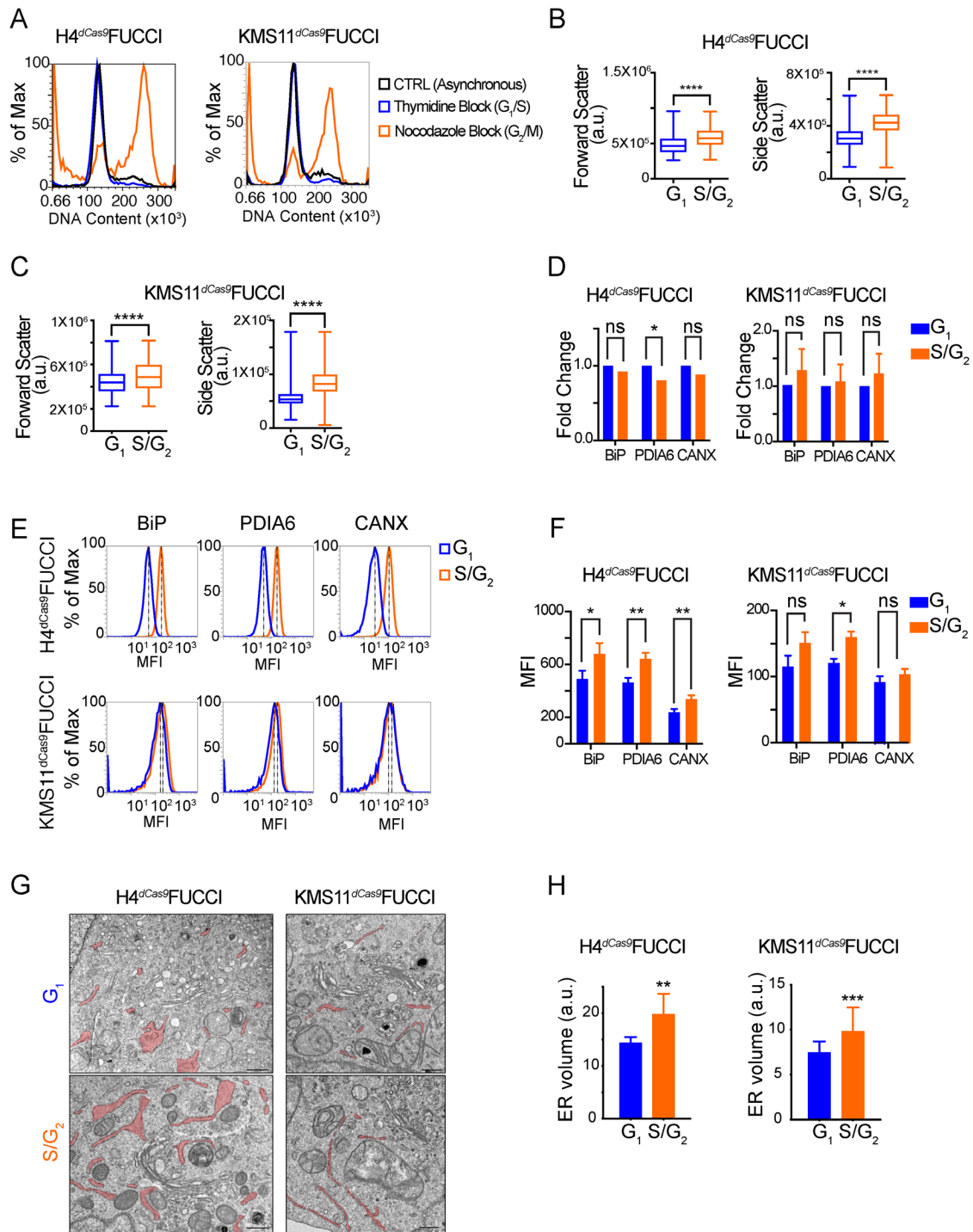


**FIGURE 2:** (A) Validation of the Fast-FUCCI system in CRISPRi H4 and KMS11 engineered cells by flow cytometry analysis of DNA content. The separation of  $G_1/S$  and  $G_2/M$  cell subpopulations was assessed upon thymidine block or nocodazole synchronization, respectively. (B and C) Side and forward scatter of asynchronous CRISPRi Fast-FUCCI cells separated by FACS according to cell cycle stage linked to the expression of the reporter. H4  $N_{G1} = 37077$ ,  $N_{G2} = 17202$ ; KMS11  $N_{G1} = 24919$ ,  $N_{G2} = 27052$ ; Paired two-tailed t test,  $***P < 0.001$ . (D) qRT-PCR analysis of ER foldase mRNA levels in asynchronous CRISPRi Fast-FUCCI cells separated by FACS as in (B and C), (H4, left; KMS11, right), normalized to *ACTB* ( $N = 3$ ; Paired two-tailed t test,  $*P < 0.05$ ). (E) Flow cytometry analysis of asynchronous CRISPRi Fast-FUCCI cells separated by FACS as in (B and C) and immunostained for BiP, PDIA6, and CANX. (F) Quantification of the data in (E). MFI: mean fluorescence intensity. ( $N = 3$ ; Paired two-tailed t test,  $**P < 0.01$ ,  $*P < 0.05$ ). (G) Representative TEM images of asynchronous  $G_1$  and  $S/G_2$  CRISPRi Fast-FUCCI cells separated by FACS as in (B and C). ER cisternae are shaded in pink. (H) Quantification of ER volume from TEM micrographs ( $N > 12$  cells; Paired two-tailed t test,  $**P < 0.01$ ,  $***P < 0.001$ ).

observed in cells not challenged by acute ER stress does not impact cell cycle dynamics to the same extent as UPR inhibition. The low levels of phosphorylated eIF2 $\alpha$  observed in unstressed cells are likely insufficient to trigger the ISR and suppress protein synthesis, which would otherwise lead to a full-blown ISR and subsequent cell cycle arrest, arising, among other factors from suppression of the synthesis of cyclin D1, as has been previously described (Brewer and Diehl, 2000; Lee *et al.*, 2019). Moreover, ISRIB treatment boosts protein synthesis (Sidrauski *et al.*, 2013), which could facilitate the oscillatory accumulation of cyclins throughout the cell cycle, promoting its timely progression and uncoupling any potential effect of eIF2 $\alpha$  phosphorylation levels on the periodicity of cyclin synthesis. Instead, our results suggest a specific role of PERK, upstream of eIF2 $\alpha$  phosphorylation, in facilitating cell-cycle progression, which challenges the previous paradigm that PERK activity inhibits the mammalian cell cycle (Brewer and Diehl, 2000; Lee *et al.*, 2019). Nevertheless, this model does not need to be reevaluated, as PERK may have different activities that satisfy suppressive or permissive roles in the cell cycle, as discussed below.

Besides itself and eIF2 $\alpha$ , PERK has been shown to phosphorylate other substrates, such as the transcription factor Nrf2 (Cullinan *et al.*, 2003), which has been proposed to be a positive regulator of the cell cycle (Lastra *et al.*, 2022). Furthermore, recent evidence indicates that PERK may play a role in phosphorylating the autophagy proteins ULK and P62, and diacylglycerol to produce phosphatidic acid, which positions PERK as a regulator of mTOR/Akt signaling—a key cell-cycle controller (Fingar *et al.*, 2004; Bobrovnikova-Marjon *et al.*, 2012; Lee *et al.*, 2022). These observations substantiate that PERK has substrates different from eIF2 $\alpha$  that could influence cell cycle timing and are consistent with our interpretation that PERK's activities independent of eIF2 $\alpha$  phosphorylation may influence cell-cycle kinetics. Our results pose an apparent dichotomy with the results of Alan Diehl, which suggest that PERK is as a negative regulator of cell cycle progression (Brewer and Diehl, 2000; Lee *et al.*, 2019). However, our results are not in conflict with this model. High PERK activity—and elevated phospho-eIF2 $\alpha$ —elicited by PERK overexpression or treatment of cells with high doses of classical ER poisons, such as thapsigargin and tunicamycin, arrests the cell cycle in G<sub>1</sub> by blocking cyclin D translation, a downstream effect of augmenting the levels of phosphorylated eIF2 $\alpha$  and suppressing global protein synthesis (Brewer and Diehl, 2000; Harding *et al.*, 2000b; Han *et al.*, 2013; Lee *et al.*, 2019). These studies highlight a potential cytoprotective role of the UPR and the ISR in responding to acute ER stress (i.e., delaying the cell cycle until the adverse conditions are mitigated). Our data, by comparison, suggest a complementary housekeeping role of PERK, outside of its canonical role in the ISR and eIF2 $\alpha$  phosphorylation, that fine-tunes cell cycle dynamics in the absence of acute ER stress. Collectively, our results and those of the Diehl lab highlight a fundamental aspect of the UPR in allowing cell decision-making concordant with physiological challenges: divide when conditions are favorable or the stress levels are tolerable, or halt cell division to refunnel resources and alleviate the stress.

Taken together, our data indicate that all three UPR branches have housekeeping functions in regulating cell-cycle dynamics. Whether canonical UPR inputs (i.e., ER protein-folding perturbations and lipid bilayer stress) or yet-to-be-discovered UPR-activating mechanisms regulate cell cycle dynamics is an outstanding question that warrants further investigation. Regardless of the activation mechanism, the UPR emerges as a link between ER expansion and cell cycle dynamics that may constitute a critical homeostatic checkpoint for maintaining the health of mitotic cells.

## MATERIALS AND METHODS

[Request a protocol through Bio-protocol.](#)

### Cell culture and drug treatments

H4 and KMS11 cells carrying the CRISPRi machinery (dCas9-KRAB; gift from Martin Kampmann, UCSF), and 293METR cells (gift from Brian Rabinovich, formerly at MD Anderson Cancer Center) were kept in DMEM (H4 and 293METR) or RPMI1640 (KMS11) supplemented with 110 mg/l sodium pyruvate, 10% fetal bovine serum (FBS), 0.1 U/ml penicillin/streptomycin, and 2 mM L-glutamine, at 37°C and 5% CO<sub>2</sub> in a humidified incubator. UPR inhibitors (5  $\mu$ M ceapin-A7 [Sigma], 500 nM ISRIB [MedChem Express], 10  $\mu$ M 4 $\mu$ 8C [MedChemExpress], and 1  $\mu$ M GSK2605414 [Adipogen Corp]) were used for 7 d in H4 cells at a seeding density of 2.5E5 cells/well in a six-well plate. To maintain drug efficacy in experiments in which we exposed H4 cells for longer than a day, all drugs were refreshed every 24 h, an interval at which cells were diluted back to the original seeding density after cell viability measurements were taken in an automated cell counter (Countess II FL, Thermo Fisher Scientific). For experiments with KMS11 cells, the seeding density was 5E5 cells/ml (KMS11), and the subculturing and cell viability measurement routine was every 48 h.

### Plasmids, lentivirus, and retrovirus production

pBOB-EF1-FAST-FUCCI-puro (gift from Kevin Brindle and Duncan Jodrell; Addgene plasmid # 86849), and pLG15 (gift of Martin Kampman, [20]) were used to express the FUCCI reporter and sgRNAs targeting IRE1, PERK, or ATF6, respectively. The sgRNA sequences were selected from the hCRISPRi-v2 library (Jonathan Weissman lab, UCSF) and cloned as previously described (Gilbert *et al.*, 2014). Retroviral constructs encoding EGFP and mCherry were built by cloning the coding sequences of the fluorescent proteins into the pLNCX2 retroviral vector (Clontech), using standard cloning methods. Lentivirus and retrovirus production was carried out as described previously (Acosta-Alvear *et al.*, 2018).

### Flow cytometry

Fast-FUCCI cell subpopulations were selected by FACS. All FACS experiments were conducted in a Sony SH800S instrument. For flow cytometry analyses, cells were fixed in ethanol or 4% paraformaldehyde at 4°C for 15 min and stained with 50  $\mu$ g/ml propidium iodide for 15 min, or with antibodies. For immunostaining, the fixed cells were resuspended in buffer FZ (50 mM NH<sub>4</sub>Cl, 0.5% bovine serum albumin (BSA), 0.05% saponin, 0.02% Na<sub>3</sub> in phosphate-buffered saline), and incubated at room temperature for 1 h. Primary (anti-BiP CST#3177, anti-Calnexin Abcam#ab22595, anti-PDI #3501) and fluorophore-conjugated secondary antibodies were diluted 1:500 in buffer FZ and incubated overnight at 4°C (primary) or 1 h at room temperature (secondary) with gentle agitation. All analyses were conducted on an Attune NxT Flow Cytometry (Thermo Fisher Scientific).

### Cell Synchronization

Cells were synchronized in G<sub>1</sub>/S using a thymidine double-block or G<sub>2</sub>/M by treating them with nocodazole after a first thymidine pulse, as previously described (Chen and Deng, 2018).

### Analysis of mitotic cells

H4 CRISPRi cells were pretreated for 4 d with UPR inhibitors and drug replenished after 48 h, labeled with 10  $\mu$ M EdU for 30 min, fixed in 4% paraformaldehyde, permeabilized with 0.25% Triton for 10 min before click-it detection, blocked in 3% BSA, and subjected

to immunostaining with antiphospho-H3 antibody (1:1000), antirabbit-Alexa594 secondary antibody (1:1000), and DAPI. Imaging was performed using a Nikon Ti-2 Eclipse inverted spinning disk confocal microscope and the micrographs were analyzed using the imaging analysis software CellProfiler (Stirling *et al.*, 2021).

### RNA extraction, cDNA synthesis, and qRT-PCR

RNA was extracted using QIAGEN's RNeasy kit according to the manufacturer's instructions. One microgram of DNaseI-treated RNA was reverse transcribed with the iScript cDNA synthesis system (BioRad) according to the manufacturer's protocol. The cDNA was diluted 10-fold in nuclease-free water and 2% was used as input for SYBR green gene-specific quantitative PCR (qRT-PCR). qRT-PCRs were carried out in a CFX96 Touch qPCR instrument (BioRad), and changes in gene expression were determined using the  $\Delta\Delta C_q$  method.

### Transmission Electron Microscopy (TEM)

Cells were fixed with 1% glutaraldehyde in 0.2 M HEPES, pH-7.3 for 30 min at room temperature and postfixed in a mixture of osmium tetroxide and potassium ferrocyanide, dehydrated in ethanol and acetone, and embedded in epoxy resin as described previously (Polishchuk and Polishchuk, 2019). Thin 60-nm sections were cut using a Leica EM UC7 ultramicrotome, and EM images were acquired using a FEI Tecnai-12 electron microscope (FEI, Eindhoven, Netherlands) equipped with a VELETTA CCD digital camera (Soft Imaging Systems GmbH, Munster, Germany). ER volume quantification was performed using iTEM software (Olympus SYS, Germany) on EM images acquired at the same magnification as follows: a 700-nm morphometric grid was applied to each image, and the number of grid nodes overlapping with ER membranes and the entire cell cytoplasm was counted. ER density was calculated by dividing the number of ER-associated nodes by the number of cytoplasm nodes. The overall ER volume was calculated for each cell as mean ER density multiplied by cytoplasm volume and expressed in arbitrary units (AU).

### Cell competition assay

GFP-labeled CRISPRi H4 cells depleted of individual UPR sensors and mCherry-labeled H4 CRISPRi cells carrying a nontargeting sgRNA control were mixed in a 1:1 ratio and diluted every 48 h to the original plating density. Samples were collected at each subculture interval for flow cytometry and microscopy analyses. Flow analyses were performed on an Attune NxT flow cytometer (Thermo Fisher Scientific) and microscopy was performed on an EchoRevolve inverted fluorescence microscope.

### EdU/PI Cell Cycle Profiling

H4 CRISPRi cells were treated with DMSO, 500 nM ISRIB, or 1  $\mu$ M GSK2606414 for 4 d and drugs replenished after 48 h. Cells were labeled for 30 min with 10  $\mu$ M EdU and released into 1  $\mu$ M nocodazole. Cell cycle profiles were analyzed immediately after labeling or after 9 h of nocodazole treatment using PI staining as described above, and flow cytometry metrics were collected in an Attune NxT flow cytometer (Thermo Fisher Scientific).

### Immunoblotting

Lysates were collected in Laemmli sample buffer, sonicated, reduced with  $\beta$ -mercaptoethanol, and boiled for 5 min before loading onto BioRad TGX Stain Free 4–20% SDS-PAGE gels and transferred onto 0.45  $\mu$ m PVDF membranes. Membranes were blocked for 1 h at room temperature with 3% BSA in 1X TRIS buffer saline Tween20 (TBST), then incubated at 4°C overnight in primary antibody solu-

tions (anti-IRE1 CST#3294, anti-PERK CST#3192 diluted 1:1000 in 3% BSA, 1X TBST), washed, and incubated for 1 h in HRP-conjugated secondary antibody solution at room temperature (diluted 1 to 5000 antirabbit in 3% BSA, 1X TBST). Immunoreactive bands were detected using SuperSignal West Femto maximum sensitivity substrate (Thermo Fisher Scientific) and a ChemiDoc MP Imaging System (BioRad).

### ACKNOWLEDGMENTS

We thank D.A.-A. lab members for insightful discussions and Adam Frost and Peter Walter for critical reading of the manuscript. This work was supported by faculty startup funds from the Department of Molecular, Cellular, and Developmental Biology, University of California, Santa Barbara (D.A.-A.) and an Otis Williams postdoctoral fellowship (UCSB) (F.Z.).

### REFERENCES

- Acosta-Alvear D, Karagöz GE, Fröhlich F, Li H, Walther TC, Walter P (2018). The unfolded protein response and endoplasmic reticulum protein targeting machineries converge on the stress sensor IRE1. *eLife* 7, e43036.
- Atxen JM, Medina JR, Feng Y, Shu A, Romeril SP, Grant SW, Li WHH, Heering DA, Minthorn E, Mencken T, *et al.* (2012). Discovery of 7-Methyl-5-(1-[[3-(trifluoromethyl)phenyl]acetyl]-2,3-dihydro-1H-indol-5-yl)-7H-pyrrolo[2,3-d]pyrimidin-4-amine (GSK2606414), a Potent and selective first-in-class inhibitor of Protein Kinase R (PKR)-like Endoplasmic Reticulum Kinase (PERK). *J Med Chem* 55, 7193–7207.
- Ayala I, Colanzi A (2017). Mitotic inheritance of the Golgi complex and its role in cell division. *Biol Cell* 109, 364–374.
- Barnum KJ, O'Connell MJ (2014). Cell cycle regulation by checkpoints. *Methods Mol Biol Clifton NJ* 1170, 29–40.
- Bicknell AA, Babour A, Federovitch CM, Niwa M (2007). A novel role in cytokinesis reveals a housekeeping function for the unfolded protein response. *J Cell Biol* 177, 1017–1027.
- Bobrovnikova-Marjon E, Pytel D, Riese MJ, Vaiteš LP, Singh N, Koretzky GA, Witze ES, Diehl JA (2012). PERK utilizes intrinsic lipid kinase activity to generate phosphatidic acid, mediate Akt activation, and promote adipocyte differentiation. *Mol Cell Biol* 32, 2268–2278.
- Bommiasamy H, Back SH, Fagone P, Lee K, Meshinchi S, Vink E, Sriburi R, Frank M, Jackowski S, Kaufman RJ, *et al.* (2009). ATF6 $\alpha$  induces XBP1-independent expansion of the endoplasmic reticulum. *J Cell Sci* 122, 1626–1636.
- Brewer JW, Diehl JA (2000). PERK mediates cell-cycle exit during the mammalian unfolded protein response. *Proc Natl Acad Sci USA* 97, 12625–12630.
- Chen G, Deng X (2018). Cell synchronization by double thymidine block. *Bio-Protoc* 8, e2994.
- Cotter L, Allen TD, Kiseleva E, Goldberg MW (2007). Nuclear membrane disassembly and rupture. *J Mol Biol* 369, 683–695.
- Cross BCS, Bond PJ, Sadowski PG, Jha BK, Zak J, Goodman JM, Silverman RH, Neubert TA, Baxendale IR, Ron D, *et al.* (2012). The molecular basis for selective inhibition of unconventional mRNA splicing by an IRE1-binding small molecule. *Proc Natl Acad Sci* 109, E869–E878.
- Cullinan SB, Zhang D, Hannink M, Arvisais E, Kaufman RJ, Diehl JA (2003). Nrf2 is a direct PERK substrate and effector of PERK-dependent cell survival. *Mol Cell Biol* 23, 7198–7209.
- Dawson TR, Lazarus MD, Hetzer MW, Wente SR (2009). ER membrane-bending proteins are necessary for de novo nuclear pore formation. *J Cell Biol* 184, 659–675.
- Fingar DC, Richardson CJ, Tee AR, Cheatham L, Tsou C, Blenis J (2004). mTOR controls cell cycle progression through its cell growth effectors S6K1 and 4E-BP1/eukaryotic translation initiation factor 4E. *Mol Cell Biol* 24, 200–216.
- Fun XH, Thibault G (2020). Lipid bilayer stress and proteotoxic stress-induced unfolded protein response deploy divergent transcriptional and non-transcriptional programmes. *Biochim Biophys Acta Mol Cell Biol Lipids* 1865, 158449.
- Gallagher CM, Garri C, Cain EL, Ang KK-H, Wilson CG, Chen S, Hearn BR, Jaishankar P, Aranda-Diaz A, Arkin MR, *et al.* (2016). Ceapins are a new class of unfolded protein response inhibitors, selectively targeting the ATF6 $\alpha$  branch. *eLife* 5, e11878.



- Gilbert LA, Horlbeck MA, Adamson B, Villalta JE, Chen Y, Whitehead EH, Guimaraes C, Panning B, Ploegh HL, Bassik MC, et al. (2014). Genome-scale CRISPR-mediated control of gene repression and activation. *Cell* 159, 647–661.
- Halbleib K, Pesek K, Covino R, Hofbauer HF, Wunnicke D, Hänel I, Hummer G, Ernst R (2017). Activation of the Unfolded Protein Response by Lipid Bilayer Stress. *Mol Cell* 67, 673–684.e8.
- Han C, Jin L, Mei Y, Wu M (2013). Endoplasmic reticulum stress inhibits cell cycle progression via induction of p27 in melanoma cells. *Cell Signal* 25, 144–149.
- Harding HP, Novoa I, Zhang Y, Zeng H, Wek R, Schapira M, Ron D (2000a). Regulated translation initiation controls stress-induced gene expression in mammalian cells. *Mol Cell* 6, 1099–1108.
- Harding HP, Zhang Y, Bertolotti A, Zeng H, Ron D (2000b). Perk is essential for translational regulation and cell survival during the unfolded protein response. *Mol Cell* 5, 897–904.
- Hollien J, Weissman JS (2006). Decay of endoplasmic reticulum-localized mRNAs during the unfolded protein response. *Science* 313, 104–107.
- Huang S, Haga Y, Li J, Zhang J, Kweon HK, Seino J, Hirayama H, Fujita M, Moremen KW, Andrews P, et al. (2022). Mitotic phosphorylation inhibits the Golgi mannosidase MAN1A1. *Cell Rep* 41, 111679.
- Karagöz GE, Aragón T, Acosta-Alvear D (2019). Recent advances in signal integration mechanisms in the unfolded protein response. *F1000Research* 8, F1000 Faculty Rev-1840.
- Koh S-B, Mascalchi P, Rodriguez E, Lin Y, Jodrell DI, Richards FM, Lyons SK (2017). A quantitative FastFUCCL assay defines cell cycle dynamics at a single-cell level. *J Cell Sci* 130, 512–520.
- KUROIWA T (2010). Mechanisms of organelle division and inheritance and their implications regarding the origin of eukaryotic cells. *Proc Jpn Acad Ser B Phys Biol Sci* 86, 455–471.
- Lastra D, Escoll M, Cuadrado A (2022). Transcription factor NRF2 participates in cell cycle progression at the level of G1/S and mitotic checkpoints. *Antioxidants* 11, 946.
- Lee A-H, Iwakoshi NN, Glimcher LH (2003). XBP-1 regulates a subset of endoplasmic reticulum resident chaperone genes in the unfolded protein response. *Mol Cell Biol* 23, 7448–7459.
- Lee D, Hokinson D, Park S, Elvira R, Kusuma F, Lee J-M, Yun M, Lee S-G, Han J (2019). ER stress induces cell cycle arrest at the G2/M phase through eIF2 $\alpha$  phosphorylation and GADD45 $\alpha$ . *Int J Mol Sci* 20, 6309.
- Lee DH, Park JS, Lee YS, Bae SH (2022). PERK prevents hepatic lipotoxicity by activating the p62-ULK1 axis-mediated noncanonical KEAP1-Nrf2 pathway. *Redox Biol* 50, 102235.
- Merta H, Carrasquillo Rodríguez JW, Anjur-Dietrich MI, Vitale T, Granade ME, Harris TE, Needleman DJ, Bahmanyar S (2021). Cell cycle regulation of ER membrane biogenesis protects against chromosome missegregation. *Dev Cell* 56, 3364–3379.e10.
- Nakajima H, Yonemura S, Murata M, Nakamura N, Piwnica-Worms H, Nishida E (2008). Myt1 protein kinase is essential for Golgi and ER assembly during mitotic exit. *J Cell Biol* 181, 89–103.
- Polishchuk EV, Polishchuk RS (2019). Pre-embedding labeling for subcellular detection of molecules with electron microscopy. *Tissue Cell* 57, 103–110.
- Puhka M, Vihinen H, Joensuu M, Jokitalo E (2007). Endoplasmic reticulum remains continuous and undergoes sheet-to-tubule transformation during cell division in mammalian cells. *J Cell Biol* 179, 895–909.
- Rhind N, Russell P (2012). Signaling pathways that regulate cell division. *Cold Spring Harb Perspect Biol* 4, a005942.
- Shibata Y, Shemesh T, Prinz WA, Palazzo AF, Kozlov MM, Rapoport TA (2010). Mechanisms determining the morphology of the peripheral ER. *Cell* 143, 774–788.
- Shibata Y, Voeltz GK, Rapoport TA (2006). Rough sheets and smooth tubules. *Cell* 126, 435–439.
- Shoulders MD, Ryno LM, Genereux JC, Moresco JJ, Tu PG, Wu C, Yates JR, Su AI, Kelly JW, Wiseman RL (2013). Stress-independent activation of XBP1s and/or ATF6 reveals three functionally diverse ER proteostasis environments. *Cell Rep* 3, 1279–1292.
- Sidrauski C, Acosta-Alvear D, Khoutorsky A, Vedantham P, Hearn BR, Li H, Gamache K, Gallagher CM, Ang KK-H, Wilson C, et al. (2013). Pharmacological brake-release of mRNA translation enhances cognitive memory. *eLife* 2, e00498.
- Sriburi R, Jackowski S, Mori K, Brewer JW (2004). XBP1: A link between the unfolded protein response, lipid biosynthesis, and biogenesis of the endoplasmic reticulum. *J Cell Biol* 167, 35–41.
- Stirling DR, Swain-Bowden MJ, Lucas AM, Carpenter AE, Cimini BA, Goodman A (2021). CellProfiler 4: Improvements in speed, utility and usability. *BMC Bioinformatics* 22, 433.
- Tam AB, Roberts LS, Chandra V, Rivera IG, Nomura DK, Forbes DJ, Niwa M (2018). The UPR activator ATF6 responds to proteotoxic and lipotoxic stress by distinct mechanisms. *Dev Cell* 46, 327–343.e7.
- Thyberg J, Moskalewski S (1998). Partitioning of cytoplasmic organelles during mitosis with special reference to the Golgi complex. *Microsc Res Tech* 40, 354–368.
- Voeltz GK, Prinz WA (2007). Sheets, ribbons and tubules - How organelles get their shape. *Nat Rev Mol Cell Biol* 8, 258–264.
- Walters AD, Bommakanti A, Cohen-Fix O (2012). Shaping the nucleus: Factors and forces. *J Cell Biochem* 113, 2813–2821.
- Yoshida H, Haze K, Yanagi H, Yura T, Mori K (1998). Identification of the cis-acting endoplasmic reticulum stress response element responsible for transcriptional induction of mammalian glucose-regulated proteins. Involvement of basic leucine zipper transcription factors. *J Biol Chem* 273, 33741–33749.